Supplementary Material:

Ultrafast Quasiparticle Dynamics and Electron-Phonon Coupling in $(Li_{0.84}Fe_{0.16})OHFe_{0.98}Se$

Qiong Wu(吴穹)[1,2], Huaxue Zhou(周花雪)[1], Yanling Wu(吴艳玲)[1], Lili Hu(胡立立)[1], Shunli Ni(倪顺利)[1,2], Yichao Tian(田义超)[1], Fei Sun(孙飞)[1,2], Fang Zhou(周放)[1,2,3], Xiaoli Dong(董晓莉)[1,2,3], Zhongxian Zhao(赵忠贤)[1,2,3], and Jimin Zhao(赵继民)[1,2,3]**

[1] *Beijing National Laboratory for Condensed Matter Physics, Institute of Physics, Chinese Academy of Sciences, Beijing 100190, China.*

[2] *School of Physical Sciences, University of Chinese Academy of Sciences, Beijing 100049, China.*

[3] *Songshan Lake Materials Laboratory, Dongguan, Guangdong 523808, China*

** *Corresponding author, Email: jmzhao@iphy.ac.cn*

1. ROTHWARF-TAYLOR MODEL

The temperature dependence of the slow component can be fully explained by the Rothwarf-Taylor model [1] and its significant extension derivations for ultrafast processes [2]. In the following, we provide details of the derivations.

The density of the thermally excited QPs n_T has a temperature dependence of [3,4]

$$n_T \propto \sqrt{\Delta(T)T}\exp\left(-\Delta(T)/k_BT\right), \tag{1}$$

where $\Delta(T)=\Delta(0)\tanh\left(\Theta\sqrt{T_c/T-1}\right)$ is the phenomenological SC gap [5,6], k_B is the Boltzmann constant, Θ is the parameter which reflects the coupling strength (which is 1.77 for weak coupling case). Here, based on our data fitting, we take Θ to be 2.02, which reveals a strong coupling in the SC state.

The Rothwarf-Taylor equation reads [1]

$$\frac{dn}{dt}=I_0+\eta N-\beta n^2, \tag{2}$$

$$\frac{dN}{dt}=J_0-\frac{\eta N}{2}+\frac{\beta n^2}{2}-\Lambda\left(N-N_T\right), \tag{3}$$

where n and N are the density of QPs and high-frequency phonons (HFPs), respectively, I_0 and J_0 are the injection terms of QPs and HFPs, respectively, η and β are the Cooper

pair breaking and formation coefficients, respectively, Λ is the rate that phonons decay into low-energy phonons or propagate away from the active region, and N_T is the density of thermally excited HFPs. Ignoring the injection terms (I_0 and J_0) and considering only the strong bottleneck case, we have at $t = t_s$

$$dn/dt = \eta N_s - \beta n_s^2 = 0, \tag{4}$$

where t_s is the time when the QPs assume their maximum density. Taking $N(t = 0) = N_T + \Delta N$ and $n(t = 0) = n_T + \Delta n$ to be the number of HFPs and QPs at the excitation by pump pulse (neither for the ground state nor for the $t = t_s$ maximum QP density point), respectively, we obtain after simple derivation that, for $t = t_s$,

$$n_s = n_T + \frac{\eta}{4\beta}\frac{\frac{16\beta}{\eta}\Delta N + \frac{8\beta}{\eta}\Delta n}{\sqrt{1+\frac{16\beta}{\eta}N_T + \frac{8\beta}{\eta}n_T}}, \tag{5}$$

Our ultrafast dynamics experiment measures the differential reflectivity, $\Delta R/R$, which is proportional to the photo-carrier density. Explicitly, we have

$$A(T) \propto n_s - n_T = \frac{\eta}{4\beta}\frac{\frac{16\beta}{\eta}\Delta N + \frac{8\beta}{\eta}\Delta n}{\sqrt{1+\frac{16\beta}{\eta}N_T + \frac{8\beta}{\eta}n_T}}, \tag{6}$$

where $A(T)$ is the amplitude of differential reflectivity in ultrafast experiment. As $n_T|_{T = 0\,K} = 0$ and $N_T \equiv (\beta/\eta)\, n_T^2$ for a steady state (see Eq. (2)), we have

$$A(0)/A(T) = 1 + 4\frac{\beta}{\eta}n_T. \tag{7}$$

Substituting Eq. (1) into Eq. (7), we can remove ΔN and Δn in Eq. (6) to obtain

$$A_{slow}(T) \propto \left[\sqrt{\Delta(T)T}\exp\left(-\Delta(T)/k_BT\right) + C\right]^{-1}, \tag{8}$$

where C is a constant containing η and β, and we have replaced $A(T)$ by $A_{slow}(T)$. Equation (8) is the fitting equation used for Fig. 2(c) in the main text, where $\Delta(0)$ and C are fitting parameters.

In parallel, regarding the lifetime, the ultrafast dynamics experiment directly measures the QP decay rate defined as $\tau^{-1} = \left|\frac{1}{n - n_T}\frac{dn}{dt}\right|_{t\to t_s}$, where τ is the lifetime of the slow component measured in our ultrafast time-resolved experiment, and n is a function of temperature that approaches n_s as t approaches t_s. During the slow process, the photo-excited QPs relax to the ground state and form Cooper pairs, accompanied by releasing of HFPs. Conversely, the HFPs can break the Cooper pairs, generating excited-state QPs. Only when HFPs decay or propagate away, will the detailed balance break. The schematic plot is shown in Fig. S1 below.

From Eqs. (2,3), after performing simple mathematical operations, we obtain

$$\frac{dn}{dt} = -2\Lambda \frac{\beta}{\eta} \frac{n^2 - n_T^2}{\frac{4\beta n_s}{\eta} + 1}. \tag{9}$$

Assuming $4\beta n_S << \eta$, we derive the following:

$$\tau \approx \frac{\eta}{2\Lambda\beta(\delta + 2n_T)}. \tag{10}$$

The temperature dependence of Λ depends on the magnitude of the SC gap as [4,7]

$$\Lambda \propto \Delta(T) + \alpha T \Delta(T)^4. \tag{11}$$

The first term corresponds to a phonon generating one lower-energy phonon (or propagating away from the active region), and the second term corresponds to a phonon generating two lower-energy phonons. Thus, the corresponding lifetime follows [7]:

$$\tau(T) \propto \left\{ \left[\delta + 2n_T(T) \right] \left[\Delta(T) + \alpha T \Delta(T)^4 \right] \right\}^{-1}, \tag{12}$$

where $\Delta(0)$, δ, and α are fitting parameters, and we have replaced $\tau(T)$ by $\tau_{slow}(T)$. Equation (12) is the fitting equation used for Fig. 2(d) in the main text. The abrupt reduction in A_{slow} and prominent increase in τ_{slow} at approximately T_c [Figs. 2(c) and (d)] are both attributed to the gradually vanishing SC gap with increasing temperature.

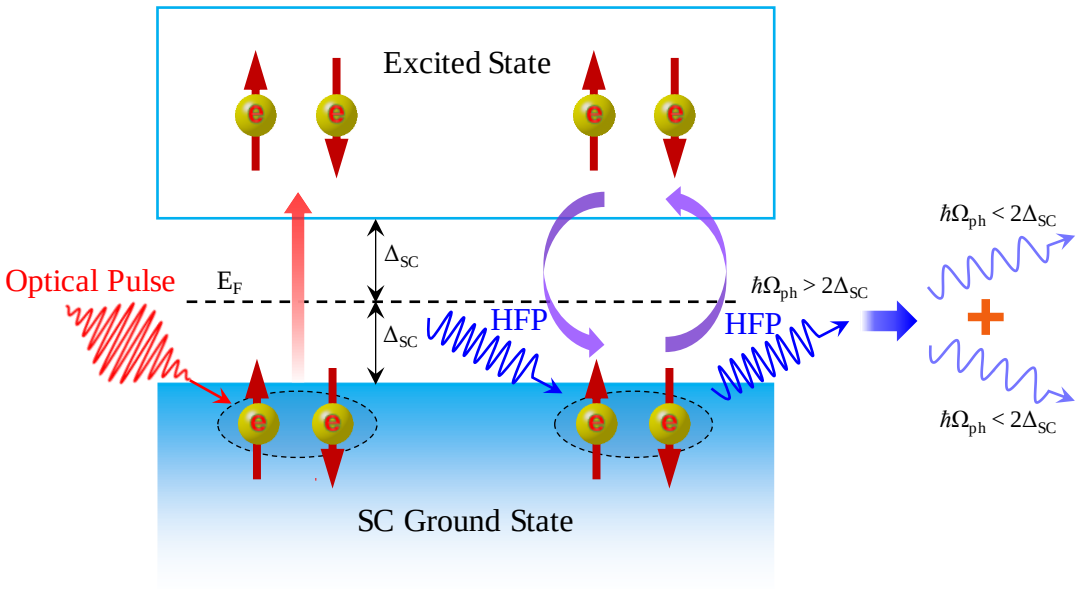

FIG. S1. Schematic of phonon-bottleneck effect in superconductors. Optical pulses break the Cooper pairs to form photo-excited QPs, which then relax and recombine to form Cooper pairs, releasing HFPs. Conversely, HFPs can break the Cooper pairs, generating excited-state QPs. This detailed balance between the QPs and HFPs only break when the HFPs decay into lower energy excitations or propagating away from the active region.

2. WEAK DETECTION CONDITION: (A) NO THERMAL EFFECT

By weak detection, we propose two different levels of criteria: (A) no thermal effect and (B) no prominent destruction of the SC component. For criterion (A), we have two aspects of verifications as follows.

2.1 Linear fluence dependence range

We measure the fluence dependence of the QP dynamics, as shown in Fig. S2(a), with the interference artifact at the so-called time-zero removed for clarity. We also measure the fluence-dependent ultrafast dynamics at several typical temperatures with fluences ranging from 4.2 to 70 μJ/cm^2 and summarize the values of $|\Delta R/R|_{max}$ obtained in Fig. S2(b) (data are offset). At all temperatures, $|\Delta R/R|_{max}$ is proportional to the laser fluence, all with a slope of 1 [Fig. S2(b)].

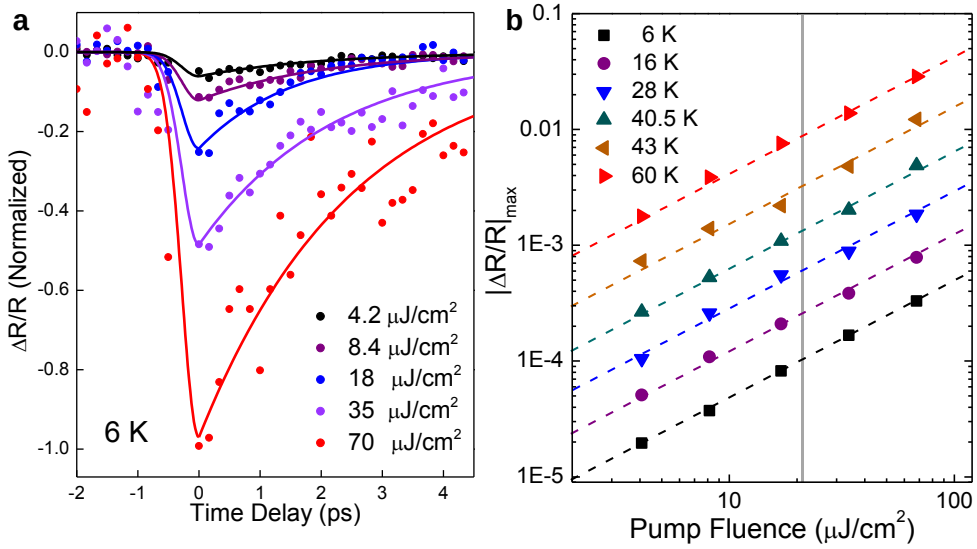

FIG. S2. Weak detection condition. (a) Fluence dependence of the differential reflectivity ($\Delta R/R$) at 6 K. Solid curves: visual guides. (b) Fluence dependence of $|\Delta R/R|_{max}$ obtained from (a) for various temperatures (offset for clarity). Dashed lines: fitting curves with a slope of 1. Gray vertical line: laser fluence used to obtain the QP dynamics data in Fig. 1 and 2 in the main text.

The fluence-dependent ultrafast dynamics that we measure [Fig. S2(a)] is also crucial in verifying that the laser pulse fluence used (21 μJ/cm^2 for pump beam) for our temperature-dependent experiment fulfills the weak detection condition criterion (A). The results in Fig. S2(b) also demonstrate that for the dynamic range of fluence, from 4.2 to 70 μJ/cm^2, the density of the photo-excited QPs is proportional to the pump fluence without saturation. Thus, the pump fluence we use (21 μJ/cm^2) to obtain the data in Figs. 1 and 2 in the main text is appropriate, without breaking the SC condensed state, or introducing extra thermal effects [8].

2.2 Less thermal effect with lower laser repetition rate

Different laser repetition rates affect the thermal effect dramatically. We compare our data with reported results. Under the same single-pulse fluence, the thermal effect is much more prominent for higher repetition rate experiments [Fig. S3]. With repetition rate increasing (from ① to ④), the ΔR/R saturation becomes more prominent, their corresponding saturation thresholds are >70 μJ/cm^2, 10 μJ/cm^2, 4.5 μJ/cm^2, and 0.8 μJ/cm^2, respectively, which is summarized in Fig. S3. It can be clearly seen that lower repetition rate allows for a much higher fluence threshold.

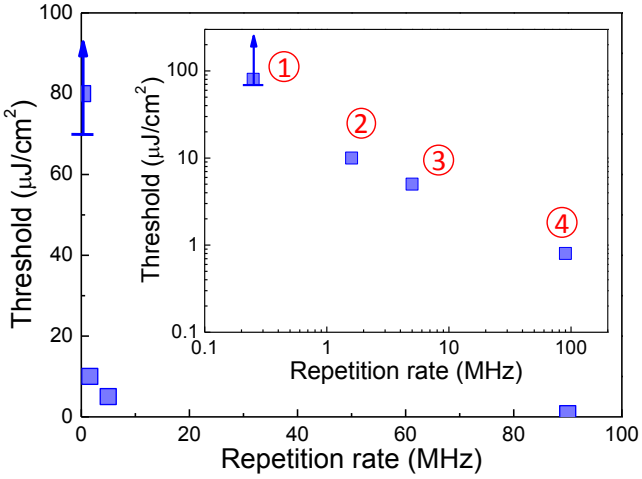

FIG. S3. Fluence threshold depending on the repetition rate. The numbers in the inset correspond to those values in this work and Refs. [9,10]. The threshold is less in an experiment with a lower repetition rate.

3. WEAK DETECTION CONDITION: (B) NO PROMINENT DESTRUCTION OF THE SC COMPONENT

To verify the fulfillment of the weak detection condition criterion (B), we estimate the fraction of electrons in the SC ground state that are photo-excited and become QPs under laser pulse incidence. Absorbed photons promote the SC ground-state electrons to the excited states, thus breaking the Cooper pairs. However, such electrons only constitute a small portion of the overall SC electrons. We estimate the fraction of such electrons within the sample as follows. Given the pump fluence $F = 21$ μJ/cm^2 and the reflectivity $R = 0.31$ (see the discussions in section 4.2), the effective pump fluence is $(1 - R)F$. After passing through one penetration depth for absorption l_s = 25 nm (see the discussions in section 4.1), the pump fluence reduces to $1/e$ times of $(1 - R)F$. The absorbed portion of the pump fluence is thus $(1 - 1/e)(1 - R)F$. Denoting the effective cross-section area of the laser spot in the sample by S, the absorbed light energy is $(1 - 1/e)(1 - R)FS$, which occurs within a volume of l_sS. Each photon generates a pair of QPs; thus, we determine the density of photo-excited QPs within a unit volume

to be

$$\rho_{QP} = 2(1-1/e)(1-R)FS/(\hbar\omega l_s S) = 3\times10^{25} m^{-3}. \quad (13)$$

Moreover, the fraction of electrons promoted to the excited state is given as

$$F_{QP} = (\rho_{QP} \times V_{uc})/unit\ cell = 3.9\times10^{-3}/unit\ cell, \quad (14)$$

where V_{uc} is the volume of the unit cell and we have taken the lattice parameters a, b, and c to be 3.7827, 3.7827 and 9.3184 Å [11], respectively. This result clearly shows that only 0.39% of the SC electrons per unit cell are excited by our pump pulses. Hence the SC ground state remains unchanged during the ultrafast dynamics investigation. We conclude that our experiment fulfills very well the weak detection condition criterion (B).

4. TEMPERATURE OF PHOTO-EXCITED ELECTRONS T_e

Immediately after the pump pulse excitation, the temperature of the photo-excited electrons T_e can be increased to as high as 10^3 K in a solid, with the lattice temperature T_L still remaining at the ambient temperature. Along the light propagation direction z, the energy density $F(z)$ experiences a simple exponential decay due to absorption:

$$F(z) = F_0 e^{-z/l_s}, \quad (15)$$

where z is the depth away from the sample surface, l_s is the penetration depth, and $F_0 = (1 - R)F$ is the energy density right at the surface. Thus, the energy transfer per volume from photons to electrons at position z is $Q(z) = -dF(z)/dz = (1/l_s)F_0 e^{-z/l_s}$. The initial electron temperature is equal to the lattice temperature $T_{ground\ state} = T_L$. Given the linear dependence of electron heat capacity C_e on electron temperature $T_{electron}$, $C_e = \kappa_v T_{electron}$, we have:

$$Q(z) = \int_{T_L}^{T_e} C_e dT_{electron} = \int_{T_L}^{T_e} \kappa_v T_{electron} dT_{electron} = (1/2)(T_e^2 - T_L^2), \quad (16)$$

Where $\kappa_v = \kappa \times \rho_n$ is the specific heat capacity coefficient per unit volume, with κ being the heat capacity coefficient and ρ_n being the mole density. Thus, we obtain

$$T_e(z) = \sqrt{T_L^2 + \frac{2(1-R)F}{\kappa_v l_s} e^{-z/l_s}}. \quad (17)$$

As T_e is a function of depth z, we consider the average T_e within one penetration depth; thus, we have:

$$T_e = \left\langle \sqrt{T_L^2 + \frac{2(1-R)F}{\kappa_v l_s} e^{-z/l_s}} \right\rangle. \quad (18)$$

4.1 Penetration depth l_s

The penetration depth of some iron-based superconductors has been reported. It is 26 nm for $Ba_{1-x}K_xFe_2As_2$ [9] and 24-26 nm for bulk FeSe [12,13]. These two different types of iron-based superconductors have similar penetration depth. Because $(Li_{0.84}Fe_{0.16})OHFe_{0.98}Se$ is an intercalated superconductor, which has similar lattice and electronic properties with those of bulk FeSe, we estimate its penetration depth to be similar to those of bulk FeSe and $Ba_{1-x}K_xFe_2As_2$. As such, we take $l_s = 25$ nm.

4.2 Reflectivity R

Measuring the reflectivity R of our sample is very challenging because the rough sample surface causes the light to diffuse in all directions, preventing the collection of the total reflected beam. We grow thin film $(Li_{0.84}Fe_{0.16})OHFe_{0.98}Se$ samples and measure its reflection at low temperatures by using 800 nm femtosecond laser pulses. The transmission of the cryostat window is taken into account. We obtain that $R = 0.31$.

4.3 Electron temperature T_e

To obtain the electron temperature T_e by Eq. (18), we use a high laser fluence F, 2.2 mJ/cm^2, and calculate T_e at a lattice temperature of $T_L = 7$ K. We have estimated that $\kappa = 100$ mJ·mol^{-1}·K^{-2} and $l_s = 25$ nm. Because in Eq. (18) $T_L^2 << \frac{2(1-R)F}{\kappa_v l_s} e^{-z/l_s}$, we have

$$T_e \approx (548.5 + \frac{T_L^2}{1074})\ K\ . \tag{19}$$

With $T_L = 7$ K, we obtain $T_e = 548.5$ K. Equation (19) can be plotted in Fig. S4. It can be seen that T_L does not affect T_e very much. At low temperature T_e is nearly a constant.

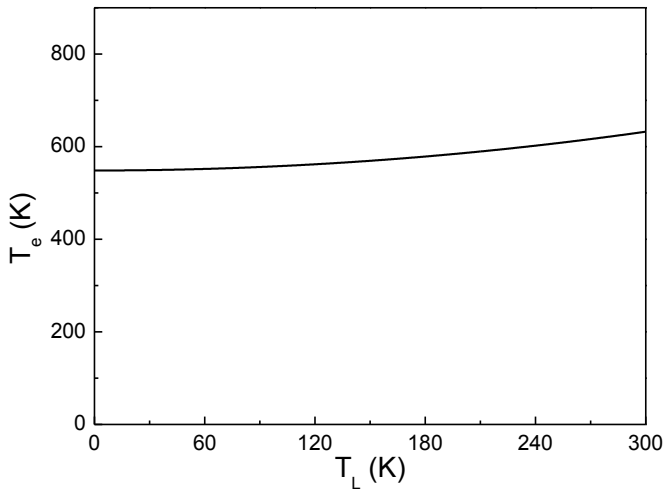

FIG. S4. The T_L dependence of T_e in $(Li_{0.84}Fe_{0.16})OHFe_{0.98}Se$. Curve plotted according to Eq. (19). It can be seen that T_e is nearly a constant at a low temperature.

5. DECONVOLUTION OF THE QP DYNAMICS

For time-resolved ultrafast spectroscopy experiments, the convolution between the QP dynamics and the excited-state accumulation response to the laser pulses occurs very often, which can lead to fake QP lifetimes. Hence de-convolution is often needed, when the pulse width is to some extent comparable to the lifetime.

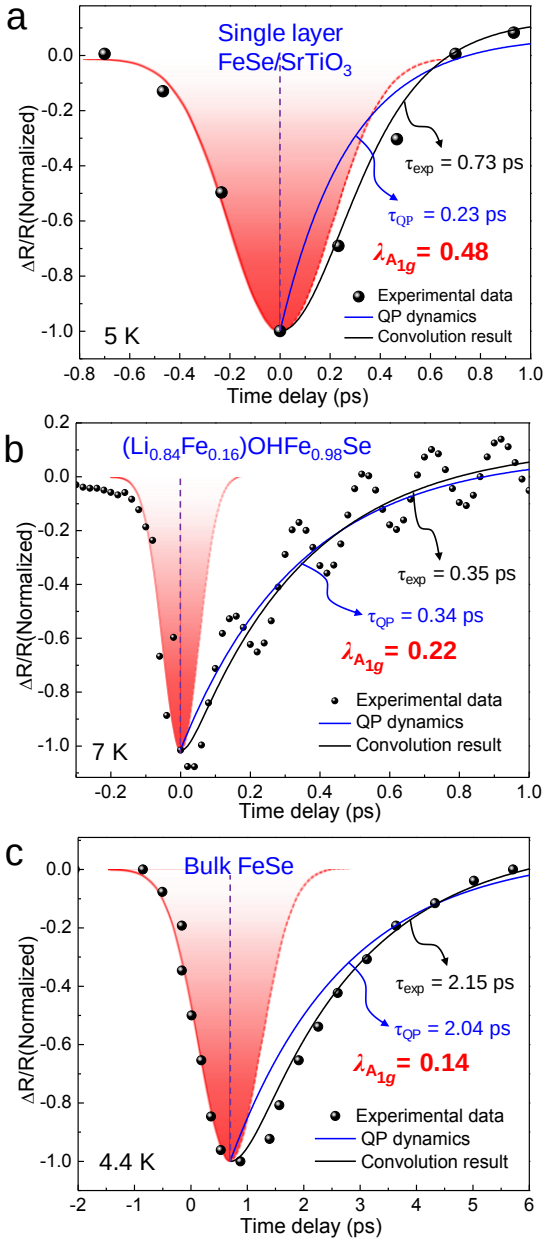

FIG. S5. Deconvolution of the QP dynamics in FeSe-based superconductors. (a) single-layer $FeSe/SrTiO_3$, (b) $(Li_{0.84}Fe_{0.16})OHFe_{0.98}Se$, (c) bulk FeSe. Black spheres: experimental data; Black curves: convolution results; Blue curves: QP dynamics; Red curves: response functions $M(t)$, where the dashed curves are the extension to construct a full Gaussian function (see text) and the vertical dashed lines mark the time-zero.

The detected signal can be expressed as

$$S(t) = D(t) \otimes M(t) = \int_{-\infty}^{+\infty} D(\tau) M(t-\tau) d\tau , \quad (20)$$

where $S(t)$ is the detected dynamics signal, $D(t) = H(t) \cdot A_{fast} \exp(-t/\tau_{fast})$ is the fast component of the QP dynamics, $H(t)$ is the unit step function, A_{fast} is the amplitude of the fast component, τ_{fast} is the lifetime of the fast component, and $M(t) = M_0 \cdot \exp(-t^2/\tau_M^2)$ is the excited state QP accumulation response to the laser pulse excitation. Although a generalization to include all relaxation components can be implemented, it is mainly the fast relaxation component that is considered, because the slow component only slightly convolutes with the response function.

We discuss the response function $M(t)$. Upon light excitation, Cooper pairs are broken to generate QPs, which experience an accumulation process. At time zero, the QPs and HFPs are $n(t = 0)$ and $N(t = 0)$. When the pair-breaking rate ηN is larger than the QP recombination rate βn^2, the QP density gradually increases even though the laser pulse has already left (see Eq. (2)) [14]. Thus, the temporal width of the response is larger than the laser pulse duration. We note that not all the accumulation process contributes to the convolution with the QP dynamics. What affects the convolution is the close-to Gaussian response function, which is contained within the accumulation process and cannot be further "reduced". We use a half-Gaussian function to fit the rising accumulation process. Because these accumulated QPs have an identical effect as an ultrafast light pulse, we then extend the response function to a full Gaussian function by adding it rear half [Fig. S5, dashed red curves]. Thus we obtain a Gaussian like response function $M(t)$ [Fig. S5]. It is this Gaussian response (not the pulse width) that convolutes with the QP dynamics. We note that the effect of the pulse duration is already contained in the response function. As examples, we de-convolute the dynamics for the three FeSe-based superconductors below.

Figure S5 shows the deconvolution for the QP dynamics of single-layer FeSe/$SrTiO_3$ (5 K, replot from Ref. [15]), $(Li_{0.84}Fe_{0.16})OHFe_{0.98}Se$ (7 K, this work), and bulk FeSe (4.4 K, replot from Ref. [16]), respectively. Ultrafast laser pulses with temporal durations of 96 fs, 70 fs, and 100 fs are used. In Fig. S5, the QP accumulation Gaussian response function has a temporal width of 490 fs, 125 fs, and 1.30 ps, respectively. In Figs. S5(a-c), the blue curves are the QPs dynamics $D(t)$, the red curves are response functions $M(t)$, and the black curves are the convolution results $S(t)$. The $S(t)$ fits well the experimental data. With such we obtain the fast component lifetimes and ultimately the EPC constants for the three materials [see Fig. S5]. We obtain the lifetimes of the fast components as 0.23 ps for single-layer FeSe/$SrTiO_3$, 0.34 ps for $(Li_{0.84}Fe_{0.16})OHFe_{0.98}Se$, and 2.04 ps for bulk FeSe. The corresponding estimated values of EPC strength $\lambda_{A_{1g}}$ are 0.48 [15], 0.22 (see below section), and 0.14, respectively.

6. OBTAINING THE EPC STRENGTH $\lambda_{A_{1g}}$

In the main text, we stated that λ can be obtained by the QP relaxation model [17] under high laser fluence excitation. This way of obtaining λ can be applied to various materials, ranging from metals to superconductors. In this model, the QP relaxation rate is determined by,

$$\gamma_T = \left(3\hbar\lambda\left\langle\Omega^2\right\rangle\Big/\pi k_B T_e\right)\left(1-\frac{\hbar^2\left\langle\Omega^4\right\rangle}{12\left\langle\Omega^2\right\rangle k_B^2 T_e T_L}+\ldots\right), \tag{21}$$

where Ω is the phonon frequency, k_B is the Boltzmann constant, and T_e is the electron temperature after photo-excitation.

6.1 Thermal relaxation rate γ_T

The thermal relaxation rate γ_T reflects the energy transfer from electron to phonons or any other types of elementary excitations, which occurs faster than that associated with phonon-phonon scattering. Thus γ_T is related to the initial decay rate in the ultrafast dynamics measurement. We plot the typical scanning traces at different temperatures ranging from 7 K to 290 K in Fig. S6. These traces are obtained with high laser fluence (see the main text for the reason). By focusing on the electronic decay rather than the superimposed oscillations, the QP lifetime at 7 K [Fig. S6(a)] can be obtained to be 0.34 ± 0.05 ps. Thus, $\gamma_T = 1/\tau_{fast} = 2.9 \pm 0.5$ ps^{-1}. We also show the temperature dependence of the QP lifetime in Fig. S6(b). It can be seen that τ_{fast} keeps nearly unchanged in the whole temperature range. This result demonstrates that the Allen model is valid in the whole temperature range for T_L (i.e. the higher order terms in Allen model can be neglected). There is a very slight decrease of the QP lifetime with temperature in Fig. S6(b). We attribute it to the subtle change of penetration depth l_s of the probe beam at different temperatures. To verify, we show the static reflectivity in Fig. S6(c), which indicates that the penetration depth is slightly smaller at room temperature, leading to a relatively lower T_e, hence smaller lifetime τ_e [Fig. S6(b)].

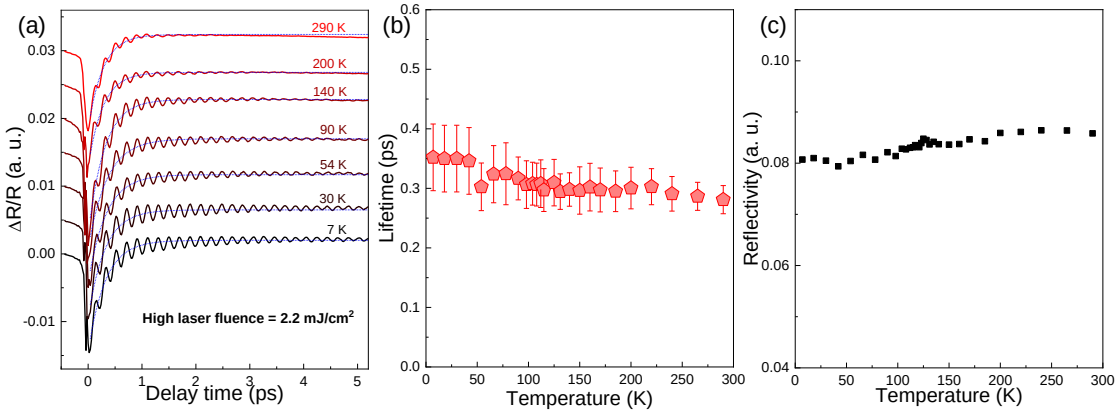

FIG. S6. Temperature dependence of the QP dynamics at 2.2 mJ/cm^2. (a) The scanning trace at several typical temperatures. The blue short-dashed curves are single-exponential fitting curves for the electronic ultrafast dynamics (fast component). (b) The temperature dependence of QP lifetime. (c) Temperature dependent static reflectivity.

A more precise way to obtain the γ_T is through the two-temperature model (TTM) described by the thermodynamics differential equations [17,18]. The exponential fitting method we use here yields equivalently accurate results, as shown in Fig. S7. In deriving the TTM *differential* result, we analyze the *difference* results for delay times. Upon approaching time zero, this yields an ideal value of γ_T, which compares excellently with the exponential fit result. This is mainly because the exponential function can fit our time-resolved experimental data very well.

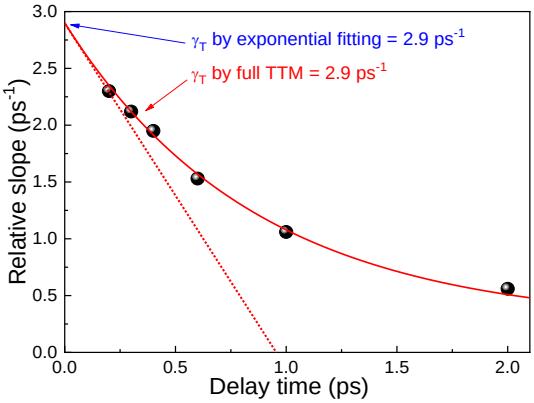

FIG. S7. Comparison of γ_T obtained by full TTM and by exponential fitting. Black sphere: slope obtained at the given delay time. Red solid curve: guide to the eyes for the trend of variation. Red dashed line: asymptotic line.

We also did the fluence dependence experiment and the result is shown in Fig. S8. In Fig. S8(a) we show the normalized dynamics data, each of which contains two components (a fast one and a slow one). To see the fast component clearly, we re-plot

a zoom-in view of the short-time region of Fig. S8(a) in Fig. S8(b). It can be seen that the fast component decays slower at higher fluences. Quantitatively, in Fig. S8(c) we summarize the lifetimes τ_{fast} as a function of fluence, which can be well fitted by a relation $\tau_{fast} = \frac{\pi k_B}{3\hbar\langle\omega^2\rangle\lambda}\sqrt{T_l^2 + \frac{2(1-R)F}{\kappa_v l_s}e^{-z/l_s}}$. This relation is derived from $\lambda = \pi k_B T_e / \left(3\hbar\langle\omega^2\rangle\tau_{fast}\right)$, (see Ref. [17]). As shown in Fig. S8(c), the estimated τ_{fast} does vary as a function of fluence, demonstrating that λ is a constant in the high fluence regime. In addition, the phonon amplitude is also illustrated in Fig. S8(d), which increases with the pump fluence.

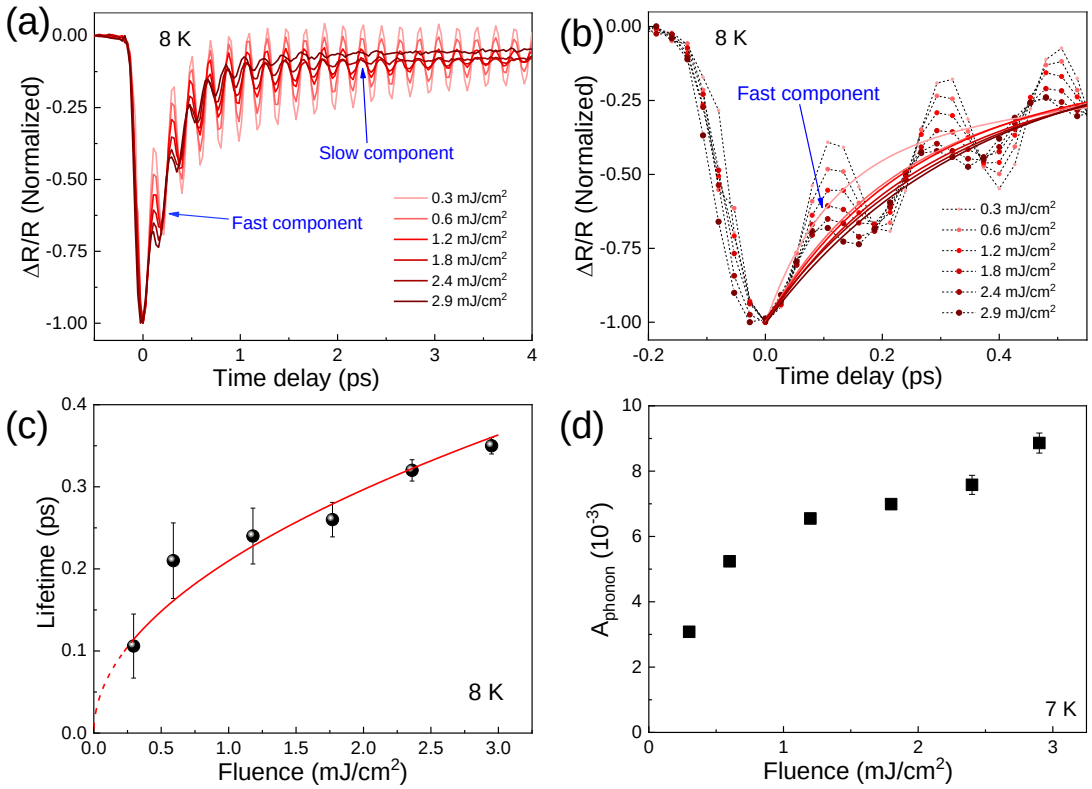

FIG. S8. Fluence dependence of τ_{fast} at relatively high fluence regime. (a) Normalized fluence-dependent QP dynamics at 8 K. (b) Zoom-in view of the fast component shown in (a). The solid curves are fittings to the dynamics other than the coherent oscillations. (c) Fluence dependence of τ_{fast} derived from (b). The dashed curve is an extension of the solid fitting curve (see text of SM). (d) Fluence dependence of phonon amplitude.

6.2 The EPC strength $\lambda_{A_{1g}}$

Given all the parameters above, we can now obtain the EPC strength λ under the condition of low lattice temperature and high laser fluence. Note that λ is a constant, which is a fundamental property that does not rely on laser fluence and persists up to a

temperature much higher than the SC T_c. As a deduction, γ_T is expected to be smaller at higher T_e, which has been verified in $Ba(Fe_{0.92}Co_{0.08})_2As_2$ [19]. As stated in the main text, we mainly consider the A_{1g} mode phonon, whose frequency is 5.11 THz (*i.e.*, 21.2 meV or 171 cm^{-1}). By Eq. (21), we obtain that $\lambda_{A_{1g}} = 0.22 \pm 0.04$, which is plotted in Fig. 4 of the main text.

7. THE T_c AND NOMINAL $\lambda_{A_{1g}}$ VALUES SHOWN IN FIG. 4

In our experiment, we measure the quantity $\langle\lambda\Omega^2\rangle$. In Allen-Dynes' treatment, the logarithmic average phonon frequency Ω_{log} is used ("with a prefactor altered from $\Theta_D/1.45$ to $\omega_{log}/1.2$") to make the McMillan equation "highly accurate" [abstract, Ref. 20]. As a reasonable treatment, we assign $\left\langle\lambda\Omega^2\right\rangle \approx \left\langle\lambda\Omega_{\log}^2\right\rangle = \lambda\Omega_{\log}^2$. Consequently, a natural and appropriate definition of the nominal $\lambda_{A_{1g}}$ is $\lambda_{A_{1g}} = \lambda(\Omega_{\log}^2 / \Omega_{A1g}^2)$, as given in the main text.

7.1 Obtaining the experimental values of $\lambda_{A_{1g}}$ shown in Fig. 4

The $\lambda_{A_{1g}}$ value of $BaFe_{1.85}Co_{0.15}As_2$ in Ref. [21] are not directly given by the authors of Ref. [21]; we extract the ultrafast dynamics result from Ref. [21], perform deconvolution, obtain the QP decay lifetime, and calculate the $\lambda_{A_{1g}}$ to be 0.125 (using the A_{1g} phonon frequency value given in Ref. [21]). Note that both [21] and our treatment here of the reported data share a similar method of obtaining $\lambda_{A_{1g}}$ as in ultrafast optical spectroscopy; hence we classify [21] into the ultrafast experiment category in Fig. 4. The lateral error bar for the bulk FeSe is given not by the authors of Ref. [16]; we extract the ultrafast dynamics result from Ref. [16], perform deconvolution, obtain the QP decay lifetime to be 2.04 ps, and derive the $\lambda_{A_{1g}}$ to be 0.14, which we set to be the lower limit of the data fluctuation. Note that the SC properties are very much sensitive to the sample-to-sample fluctuation for bulk FeSe.

Furthermore, we perform an additional experiment on two other iron-based superconductors, respectively. We grow two nearly optimized samples: $Fe_{1.05}Se_{0.2}Te_{0.8}$ (T_c = 10 K) and $Fe_{1.01}Se_{0.2}Te_{0.8}$ (T_c = 13.5 K). The pump fluence is 16 $\mu J/cm^2$, which is nearly identical to that in Ref. [16], where the photon energy is 1.55 eV for pump and probe beam. We measure the dynamics at 10 K, as shown in Fig. S9. A fast component with a lifetime of a few hundreds of fs is clearly detected in both two samples. For $Fe_{1.05}Se_{0.2}Te_{0.8}$, the fast component lifetime is 0.31 ± 0.05 ps, and for $Fe_{1.01}Se_{0.2}Te_{0.8}$ the fast component lifetime is 0.27 ± 0.05 ps. By using Allen model and similar treatment in Ref. [16], we identify the $\lambda_{A_{1g}}$ values of $Fe_{1.05}Se_{0.2}Te_{0.8}$ and $Fe_{1.01}Se_{0.2}Te_{0.8}$ to be 0.11 ± 0.03 and 0.13 ± 0.03, respectively.

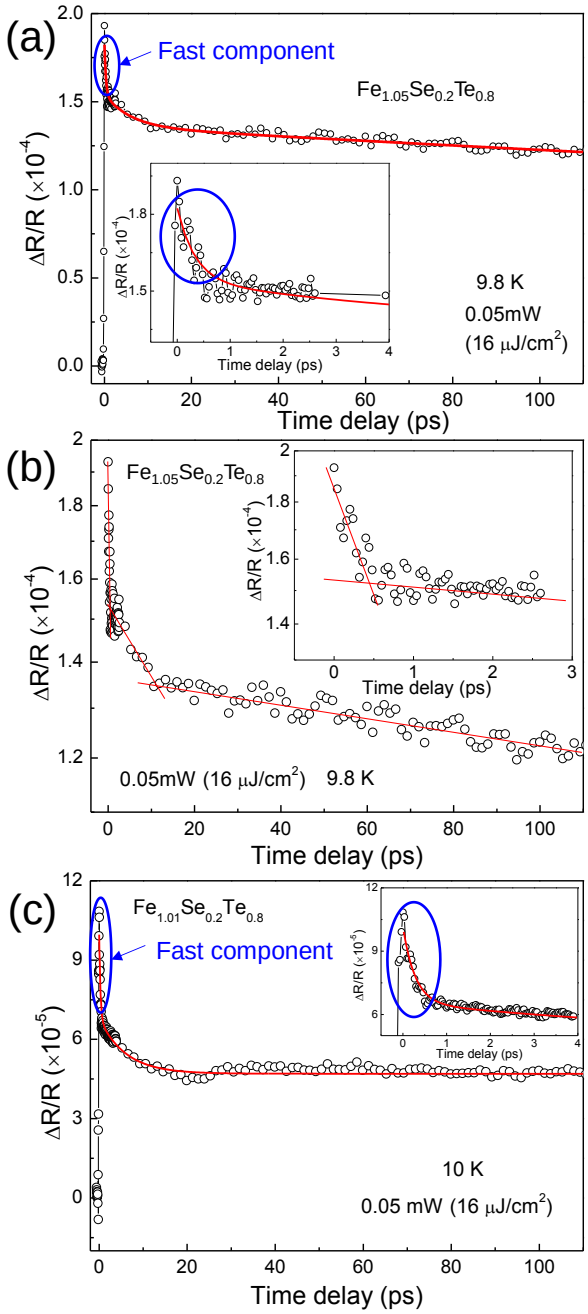

FIG. S9. Ultrafast dynamics of $Fe_{1.05}Se_{0.2}Te_{0.8}$ and $Fe_{1.01}Se_{0.2}Te_{0.8}$. (a) The scanning trace of $Fe_{1.05}Se_{0.2}Te_{0.8}$ at 9.8 K. (b) The y-axis logarithmic scale plot of the same data shown in (a). The red solid lines are guides to the eyes for the multi-components of the dynamics. (c) The scanning trace of $Fe_{1.01}Se_{0.2}Te_{0.8}$ at 10 K. The red solid curves in (a) and (c) are fitting curves with multi-exponential functions. The inset figures are zoom-in views. The fast components are marked by blue circles.

7.2 Retrieving the theoretical values of $\lambda_{A_{1g}}$ shown in Fig. 4

In Fig. 4 of the main text, the $\lambda_{A_{1g}}$ values of LiFeAs [22], NaFeAs [22], $CaFe_{1.85}Co_{0.15}As_2$ [23], $K_xFe_2Se_2$ [24], $Ba_{0.6}K_{0.4}Fe_2As_2$ [25], and $FeSe_{0.5}Te_{0.5}$ [26] superconductors were not reported by their authors, but are retrieved from the

references by us. In these references, the theoretical λ values are calculated based on the Eliashberg function using the logarithmic average phonon frequency Ω_{log} (Table 1). The average phonon frequency Ω_{log} and the A_{1g} phonon frequency $\Omega_{A_{1g}}$ were also reported (Table 1). Given that $\lambda \propto 1/\langle\Omega^2\rangle$ [27], to the first order of approximation, we retrieve the values of $\lambda_{A_{1g}}$ by using $\lambda_{A_{1g}} = \lambda(\Omega_{log}^2/\Omega_{A_{1g}}^2)$.

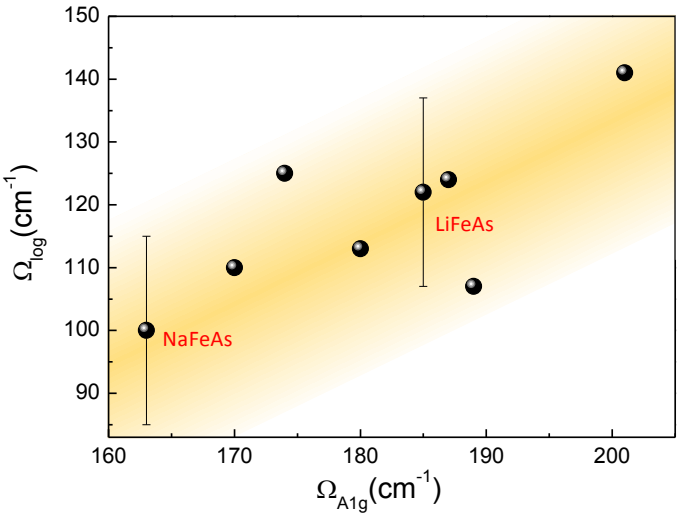

FIG. S10. Estimation of the Ω_{log} value of LiFeAs and NaFeAs. Yellow stripe: overall positive correlation between $\Omega_{A_{1g}}$ and Ω_{log}.

For LiFeAs and NaFeAs, their Ω_{log} values have not been reported. We estimate it by the following way. We illustrate the $\Omega_{A_{1g}}$ vs Ω_{log} of Fe-based superconductors in below Fig. S10. It can be seen that the Ω_{A1g} and Ω_{log} values have a positive correlation (the yellow stripe). We assume that LiFeAs and NaFeAs also obey this correlation. From the plot, we can obtain the Ω_{log} of LiFeAs is 120 ± 15 cm^{-1} and that of NaFeAs is 100 ± 15 cm^{-1}. Thus the corresponding $\lambda_{A_{1g}}$ values are obtained to be 0.12 and 0.1, respectively. Thus, we obtain the values of $\lambda_{A_{1g}}$ (Table 2). We emphasize that all the cited theoretical works in Fig. 4 use the same definition of λ following Allen, and the experimental data all rely on the ultrafast dynamics described by the Allen model.

The pink curve in Fig. 4 is a modified Allen-Dynes formula, where λ is replaced by $6.5\lambda_{A_{1g}}$, and Ω_{log} by $1.5\Omega_{A_{1g}}$:

$$T_c = \frac{1.5\Omega_{A_{1g}}}{1.2}\exp\left[-\frac{1.04\left(1+6.5\lambda_{A_{1g}}\right)}{6.5\lambda_{A_{1g}} - \mu^*\left(1+0.62\times 6.5\lambda_{A_{1g}}\right)}\right]. \quad (22)$$

To the first order of approximation, we specify an average value of $\Omega_{A_{1g}}$ for the various materials. We choose 176 cm^{-1} (i.e., 21.8 meV), where in Fig. 4 the smallest value is 163 cm^{-1} (for NaFeAs) and the largest is 189 cm^{-1} (for $CaFe_{1.85}Co_{0.15}As_2$). The orange curve is another modified Allen-Dynes formula, with λ replaced by 2.7λ and Ω_{log} replaced by $2.31\Omega_{log}$:

$$T_c = \frac{2.31\Omega_{\log}}{1.2}\exp\left[-\frac{1.04(1+2.7\lambda)}{2.7\lambda-\mu^*(1+0.62\times 2.7\lambda)}\right]. \quad (23)$$

Similarly, we specify an average value of $\Omega_{\log}$ to be 120 cm^{-1} (i.e., 14.9 meV). Similar to the treatments for conventional superconductors, $\mu^* = 0.1$ is used in both equations.

8. AFFECTING THE EPC THROUGH MODIFING THE ELECTRONIC STATES, PHONONS, OR BOTH

For the discussion (the first paragraph of the discussion section) in the main text, we provide an illustration here as a possible example.

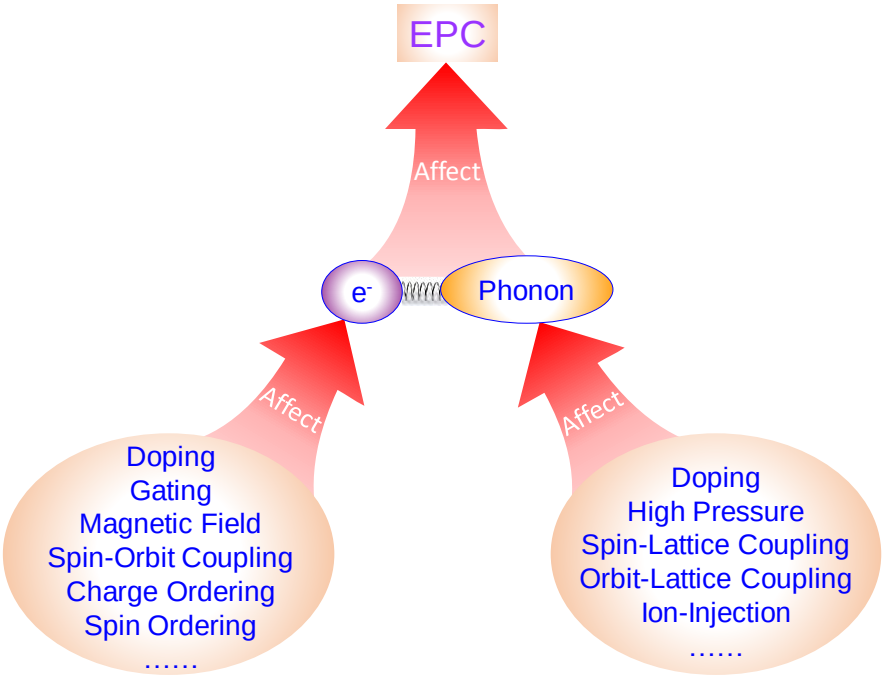

FIG. S11. The EPC can be affected by modifications in the electronic states, phonons, or both. The electronic states can be affected by doping, gating, magnetic field, spin ordering, charge ordering, spin-orbit coupling, *etc.*; the phonons can be affected by doping, high pressure, spin-lattice coupling, orbit-lattice coupling, ion injection, *etc.*

References

[1] Rothwarf A and Taylor B N, 1967 Phys. Rev. Lett. **19**, 27

[2] Kabanov V V, Demsar J, and Mihailovic D, 2005 Phys. Rev. Lett. **95**, 147002

[3] Aronov A G and Spivak B Z, 1977 J. Low Temp. Phys. **29**, 149

[4] Kabanov V V, Demsar J, Podobnik B, and Mihailovic D, 1999 Phys. Rev. B **59**, 1497

[5] Senapati K, Blamire M G, and Barber Z H, 2011 Nat. Mater. **10**, 849

[6] Wang Z S, Wang Z Y, Luo H Q, Lu X Y, Zhu J, Li C H, Shan L, Yang H, Wen

H H, and Ren C, 2012 Phys. Rev. B **86**, 060508
[7] Chia E E M, Zhu J X, Lee H J, Hur N, Moreno N O, Bauer E D, Durakiewicz T, Averitt R D, Sarrao J L, and Taylor A J, 2006 Phys. Rev. B **74**, 140409
[8] Giannetti C, Coslovich G, Cilento F, Ferrini G, Eisaki H, Kaneko N, Greven M, and Parmigiani F, 2009 Phys. Rev. B **79**, 224502
[9] Torchinsky D H, McIver J W, Hsieh D, Chen G F, Luo J L, Wang N L, and Gedik N, 2011 Phys. Rev. B **84**, 104518
[10] Gedik N, Langner M, Orenstein J, Ono S, Abe Y, and Ando Y, 2005 Phys. Rev. Lett. **95**, 117005
[11] Dong X L, Jin K, Yuan D N, Zhou H X, Yuan J, Huang Y L, Hua W, Sun J L, Zheng P, Hu W, Mao Y Y, Ma M W, Zhang G M, Zhou F, and Zhao Z X, 2015 Phys. Rev. B **92**, 064515
[12] Luo C W, Wu I H, Cheng P C, Lin J Y, Wu K H, Uen T M, Juang J Y, Kobayashi T, Chareev D A, Volkova O S, and Vasiliev A N, 2012 Phys. Rev. Lett. **108**, 257006
[13] Wen Y C, Wang K J, Chang H H, Luo J Y, Shen C C, Liu H L, Sun C K, Wang M J, and Wu M K, 2012 Phys. Rev. Lett. **108**, 267002
[14] Demsar J, Averitt R D, Taylor A J, Kabanov V V, Kang W N, Kim H J, Choi E M, and Lee S I, 2003 Phys. Rev. Lett. **91**, 267002
[15] Tian Y C, Zhang W H, Li F S, Wu Y L, Wu Q, Sun F, Zhou G Y, Wang L L, Ma X C, Xue Q K, and Zhao J M, 2016 Phys. Rev. Lett. **116**, 107001
[16] Luo C W, Wu I H, Cheng P C, Lin J Y, Wu K H, Uen T M, Juang J Y, Kobayashi T, Wen Y C, Huang T W, Yeh K W, Wu M K, Chareev D A, Volkova O S, and Vasiliev A N, 2012 New J. Phys. **14**, 103053
[17] Allen P B, 1987 Phys. Rev. Lett. **59**, 1460
[18] Anisim ov S I, Kapeliovich B L, and Perelman T L, 1974 Sov. Phys.-JETP **39**, 776
[19] Mansart B, Boschetto D, Savoia A, Rullier-Albenque F, Bouquet F, Papalazarou E, Forget A, Colson D, Rousse A, and Marsi M, 2010 Phys. Rev. B **82**, 024513
[20] Allen P B and Dynes R C, 1975 Phys. Rev. B **12**, 905
[21] Avigo I, Cortes R, Rettig L, Thirupathaiah S, Jeevan H S, Geogenwart P, Wolf T, Ligges M, Wolf M, Fink J, and Bovensiepen U, 2013 J. Phys. Cond. Mat. **25**, 094003
[22] Jishi R A and Alyahyaei H M, 2010 Adv. Cond. Matter. Phys. **2010**, 804343
[23] Miao R D, Bai Z, Yang J, Chen X, Cai D, Fan C H, Wang L, Zhang Q L, and Chen L A, 2013 Solid State Commun. **154**, 11
[24] Bazhirov T and Cohen M L, 2012 Phys. Rev. B **86**, 134517
[25] Boeri L, Calandra M, Mazin I I, Dolgov O V, and Mauri F, 2010 Phys. Rev. B **82**, 020506
[26] Li J and Huang G Q, 2013 Solid State Commun. **159**, 45
[27] Mcmillan W L, 1968 Phys. Rev. **167**, 331